http://dx.doi.org/10.21577/0103-5053.20190154

J. Braz. Chem. Soc., Vol. 31, No. 1, 175-185, 2020
Printed in Brazil - ©2020 Sociedade Brasileira de Química

Article

Microwave Assisted Ultra-Fast Method to Synthesize Carbonate-Phosphates, $Na_3MCO_3PO_4$ (M = Mn, Fe, Co, Ni) - Relevant Materials Applied in Sodium-Ion Batteries

Demétrio A. S. Costa, [a,b] ***Lorena A. C. Costa,*** [a] ***João O. Mendes,*** [a] ***Wagner N. Mussel,*** [a] ***José D. Ardisson*** [c] ***and Luciano A. Montoro**,*** [a]

[a]*Departamento de Química, Instituto de Ciências Exatas, Universidade Federal de Minas Gerais, 31270-901 Belo Horizonte-MG, Brazil*

[b]*Colégio Técnico (COLTEC), Universidade Federal de Minas Gerais, 31270-901 Belo Horizonte-MG, Brazil*

[c]*Centro de Desenvolvimento da Tecnologia Nuclear, 31270-901 Belo Horizonte-MG, Brazil*

Although largely used in mobiles and electric vehicles applications, insertion batteries based on Li-ion technology are high-cost devices. These applications require high-performance energy storage systems with high-energy and high-power densities, which are better attained by Li-ion technology. However, stationary applications such as power plants and uninterruptible power supplies (UPS) mainly require low-cost energy storage devices. In this scenario Na-ion insertion batteries feature as a cheaper option for such applications. Among the several compounds for use as cathode in Na-batteries, a largely studied class of compounds are the sodium-carbonate-phosphates, $Na_3MCO_3PO_4$ (M = Mn, Fe, Co or Ni), with structure analogue to the mineral sidorenkite. In this work, it was developed a new microwave-assisted hydrothermal method as an ultra-fast way to prepare sodium-carbonate-phosphate compounds. This methodology results in high-quality materials with general formula $Na_3MCO_3PO_4$ (M = Mn, Fe, Co or Ni) upon only 5 min processing time. Characterization techniques indicate highly ordered materials with sidorenkite-like phase and different morphologies or crystal habits, including plates, rods, and a 'starfruit' shape. As a proof-of-application the Mn-based material was evaluated from electrochemical tests for Na^+ insertion reactions. The obtained results evidence initial discharge capacity of 107 mA h g^{-1} with good reversible capacity (65 mA h g^{-1}) after several charge/discharge cycles.

Keywords: sidorenkite, sodium-ion insertion, microwave, solvothermal method

Introduction

Modern portable electronic devices and electrical/hybrid vehicles require high energy performance batteries. This high performance is associated with high-energy capacity and/or high-power density, combined to a long cycle life. These features can be better attained by the modern lithium ion batteries, where improvements on electrode materials and cell engineering has pushed it up to a state-of-the-art energy storage. However, a critical drawback for large scale Li-ion battery application is the high cost associated with the cell components (electrode materials, high-purity electrolyte, separator) added to the cost of the pack assembly. Thus, in order to reduce the cost of the cell components a good approach is the replacement of the lithium and cobalt compounds. Lithium is expensive, where the actual resources are evenly distributed across the planet and requires large amounts of drinking water for extraction and production. A good alternative for production of low-cost devices are the intensively studied sodium-ion batteries. Sodium is inexpensive and abundant on the Earth's crust.[1-3] Nowadays, several works[4-8] suggest that batteries based on sodium ion hold promise as a potential alternative to replace lithium-based technology.

For the development of Na-batteries it is necessary to find new materials for ion insertion electrodes. Different materials have been developed and studied along last years, and the sodium-carbonate-phosphates, $Na_3MCO_3PO_4$ (M = M^{2+} transition metals), are a class of materials that have received attention due to its good electrochemical performance and the low-cost associated with the constituent elements, Na and Mn.[9] Those elements

*e-mail: montoro@ufmg.br

are used to prepare the $Na_3MnCO_3PO_4$, the most studied sodium-carbonate-phosphate.[3,10-13] This compound is often denominated as sidorenkite, the mineral form of the $Na_3MnCO_3PO_4$. When applied to Na-batteries, this material shows a high theoretical specific capacity of 191 mA h g^{-1} that comes from the two involved redox pairs during charge and discharge cycles, Mn^{2+}/Mn^{3+} and Mn^{3+}/Mn^{4+}.[14] In addition, other transition metals such as cobalt, iron or nickel can also be used, resulting in different sidorenkite analogue materials for Na-batteries ($Na_3MCO_3PO_4$, M = Mn, Fe, Co, Ni).

These sidorenkite materials can be used as active materials for electrodes in Na^+ ion batteries, where Na^+ ions can be reversibly inserted and deinserted from electrochemical reactions. The Na-battery works through a mechanism similar to a Li-battery, where the Na^+ extraction/insertion from/into the material's structure occurs as a result of the oxidation/reduction of the transition metals.[13,15,16] Problems associated with the use of Na ions instead Li include the less negative redox potential, reducing the cell voltage and the higher Na molar mass, which results in a lower specific energy capacity.[17,18] In addition, the larger ionic radii of the Na-ion lead to a lower ionic diffusion through the material's structure and, consequently, decrease the charge/discharge rates. However, the sodium abundance and the low cost associated with the active materials, contribute to do Na-ion batteries competitive devices in replacement of the current Li-ion technology for large scale applications, such as in stationary systems.[16,19,20]

The production methods applied for material's preparation are often based on solid state reactions from coprecipitates or sol-gel precursors. These materials can be produced by thermal heating methods at a relatively low energy cost.[21,22] In the specific case of the sodium-carbonate-phosphates the reported methods[9,21,23-25] are based on hydrothermal processing of a precursor mixture inside autoclaves at moderate temperatures but with a long processing time, during a few days or a week. A good strategy to improve these time demanding methods in order to reduce processing time is associated to the use of microwave heating.[26-34] Solvothermal methods based on microwave-assisted processing have been largely explored for preparation of a variety of different materials.[24,34-37] Microwave-assisted solution methods are an efficient approach for nanomaterials synthesis with additional advantages as compared to other methods, such as the rapid volumetric heating, high reaction rate, a better size and shape control of nanoparticle formation, and good energy efficiency. Moreover, the homogeneous heating provided by microwave processing minimizes thermal gradients resulting in uniform nucleation and growth that leads to nanoparticles with more uniform size and shape.[38] Thus, by using a microwave processing one can achieve more efficient methods for battery materials preparation in an energy saving and low-cost approach.[30,35,36,39]

In the present work, the use of a microwave-assisted method for the preparation of sodium-carbonate-phosphates $Na_3MCO_3PO_4$ (M = Mn, Fe, Co, Ni) was investigated as a promising methodology to prepare high-quality materials. The goal of this work is the attainment of an efficient method to prepare relevant materials with a good control of crystallinity, particle size and morphology, in an ultra-fast way.

Experimental

The materials were synthesized from a mixture of precursor salts containing the constituent metals and anions, carbonate and phosphate. In a typical procedure 6.66×10^{-3} mol of Mn^{2+}, Fe^{2+}, Co^{2+} or Ni^{2+} as a metal salt was dissolved in 15.0 mL of deionized water. The metal salts were acetates for Mn, Co and Ni, $M(C_2H_3O_2)_2.4H_2O$ (Synth, Diadema, Brazil), and a chloride for Fe, $FeCl_2.4H_2O$ (Sigma-Aldrich, São Paulo, Brazil). In 45.0 mL of deionized water were dissolved 0.945 g of Na_2HPO_4 (Neon, São Paulo, Brazil) and 6.667 g of Na_2CO_3 (Synth, Diadema, Brazil). The transition metal solution was dropwise added to the sodium salts solution and then sealed in a Teflon/PEEK (polyetheretherketone) reactor for microwave processing. It was used a microwave oven with controlled temperature and processing time (Milestone, Start D). To evaluate the microwave processing for obtaining the desired sidorenkite compounds, different temperatures, 120, 150, 180 and 210 °C were used at a constant processing time of 30 min. Additionally, the Mn-based precursor mixture was microwave processed in a constant temperature of 210 °C at different processing times, 5, 10 and 20 min. After each reaction the resulting material was filtered and washed with abundant water and ethanol. The solid products were then dried under vacuum in a desiccator for 24 h.

The powder X-ray diffraction (XRD) patterns were obtained in a Shimadzu equipment model XRD-7000 X-ray using CuKα radiation. The cell parameters were determined by the Rietveld refinement method using the software Fullprof.[40] Scanning electron microscopy (SEM) analyses were carried out in a FEI Quanta 200 FEG by using secondary electron detection and 30 kV of acceleration voltage. Thermal analyses (TGA) were performed in a Shimadzu DTG 60H with an Ar flow of 30 mL min^{-1} at a heating rate of 10 °C min^{-1} up to 700 °C. The thermogravimetric analysis coupled to mass-spectrometry (TGA-MS) was performed in a Netzsch equipment model

STA 449 F3 with an Ar flow of 30 mL min^{-1} at a heating rate of 10 °C min^{-1} up to 700 °C. The Mössbauer spectrum of ^{57}Fe was acquired in a CMTE spectrometer model MA250 with constant acceleration by moving a ^{57}Co source into a Rh matrix.

The electrochemical characterization was performed in a three-electrode cell connected to a Bio-Logic VMP-300 multipotentiostat, using an Ag|AgCl (3 M) reference electrode. The specific energy capacity was evaluated from a galvanostatic charge/discharge method (chronopotentiometry) by using different charge/discharge rates (C-rates). Considering a theoretical capacity of 191 mA h g^{-1}, four charge/discharge cycles were performed consecutively at C/20, C/4, C/2, C, 2.5C, 5C, returning to C/20. The used electrolyte was a 0.5 mol L^{-1} sodium sulfate, Na_2SO_4 (Synth, Diadema, Brazil) aqueous solution. The working electrode (WE) was prepared from a mixture of the 70 wt.% active material, 10 wt.% polyvinylidene fluoride (PVDF, Solef 1012, Solvay, Hannoven, Germany) and 20 wt.% carbon black (Erachem, Europe MMM Carbon, Willebroek, Belgium), in 2.0 mL of *N*-methyl pyrrolidinone (Merck, Hohenbrunn, Germany). This mixture was submitted to vortex agitation (with glass beads in a small bottle) for 2 min and ultrasonic irradiation for 10 min. The obtained slurry was deposited onto a carbon cloth (Fuel Cell Earth, CC4 plain) by using a doctor blade and the electrode was dried for a few hours at 70 °C. A similar procedure was applied to prepare the counter electrode (CE) by using a copper hexacyanoferrate as active material. This material shows a proven reversible Na insertion capability.

Results and Discussion

Figure 1 shows the XRD acquired for the obtained materials with 30 min of processing time at temperatures ranging from 120 to 210 °C. These results indicate that the

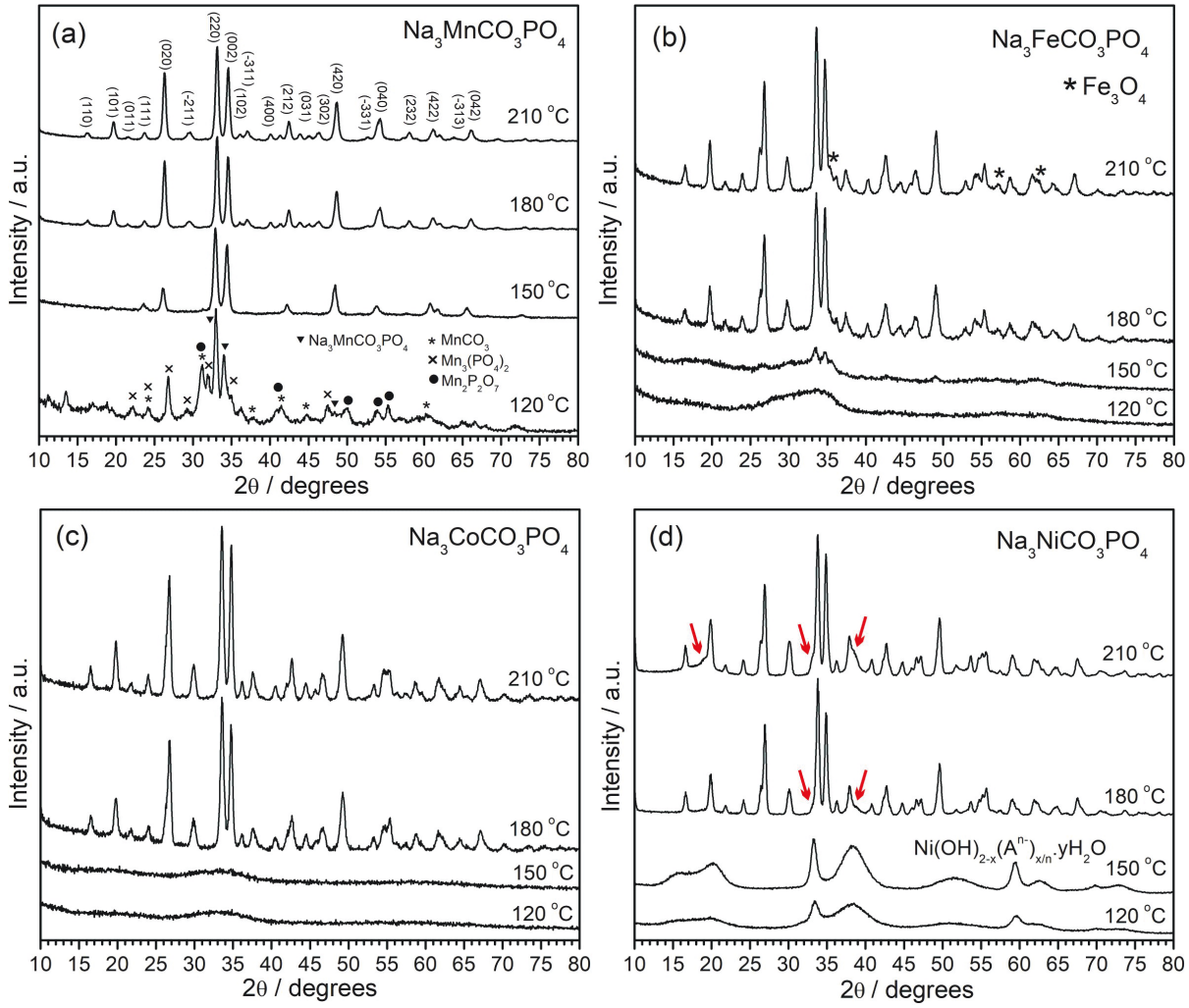

Figure 1. X-ray diffraction patterns of the obtained materials upon processing the reactional mixtures during 30 min at temperatures of 120, 150, 180 and 210 °C. (a-d) Results for the Mn-, Fe-, Co- and Ni-based compounds, respectively. The red arrows indicate peaks attributed to the formation of the layered nickel hydroxide phase.

sodium-carbonate-phosphate phases $Na_3MCO_3PO_4$ were obtained in a highly ordered state. The Mn-sidorenkite pattern (Figure 1a) can be accordingly indexed in a monoclinic phase with $P2_1/m$ space group (PDF 084-0023). In addition, the Fe, Co and Ni sidorenkite-analogue compounds are isostructural phases and show the same diffraction pattern with slight modifications at peak positions, evidencing variations of lattice spacings induced by the different M^{2+} ionic radii. From Figure 1a it is possible to infer that temperatures above 150 °C are necessary to result the single Mn-sidorenkite phase. A microwave processing at 120 °C results in a mixture of different insoluble Mn compounds, mainly including manganese carbonate, manganese phosphate and manganese pyrophosphate. However, the sidorenkite formation is also evidenced by the two main peaks (220) and (002). It was previously reported that the Mn-sidorenkite material can be synthesized from a similar precursor mixture processed at 120 °C in a hydrothermal autoclave reactor with conventional heating. Although, an efficient synthesis was only achieved by using a long processing time of 20 h to produce a good crystallinity material.[9]

Figure 1b shows the XRD patterns of the iron-based compounds processed at different temperatures. These diffraction patterns evidence formation of a single Fe-sidorenkite crystalline phase only above 180 °C. Below this temperature it was obtained very low crystallinity materials with no relevant diffraction peaks evidencing the resulting phases. However, at 150 °C it is possible to observe some very low intensity peaks which can be attributed to the $Na_3FeCO_3PO_4$ phase. It is worth noting that the $Na_3FeCO_3PO_4$ compounds obtained above 180 °C seems to be contaminated with a small amount of the iron oxide Fe_3O_4, as evidenced by the indicated peaks (Figure 1b). This side phase can be resulted from iron(II) oxidation by the oxygen and water present in the reaction vessel.

Figure 1c evidences very similar results for the Co-sidorenkite phase $Na_3CoCO_3PO_4$, where the use of temperatures above 180 °C results in high crystalline materials with no side products. Amorphous, or very low crystallinity compounds were obtained at 150 and 120 °C.

The diffraction patterns of the Ni-based compounds (Figure 1d) reveal that two distinct compounds were obtained. At high temperatures, 180 and 210 °C, highly crystalline $Na_3NiCO_3PO_4$ were obtained. On the other hand, by using low temperatures, 120 and 150 °C, it was obtained a layered nickel α-hydroxide, $Ni(OH)_{2-x}(A^{n-})_{x/n}.yH_2O$. This is a hydroxyl-deficient compound which incorporates anions, PO_4^{3-} and CO_3^{2-}, in its interlamellar region.[41] A previous work[9] reported similar results during $Na_3NiCO_3PO_4$ synthesis, but this side product was not properly identified.

In addition, an interesting feature to be analyzed is the periodic trend related to the carbonate-phosphate formation. From these XRD results one can observe that the Mn-based compound was already formed at 150 °C. Whereas at 150 °C, the Fe compound formation was faintly evidenced by the two weak diffraction peaks (220) and (002) and the Co- and Ni-based sidorenkite compounds were only formed at higher temperatures, with no evidence of such phases at 150 °C. This observed trend follows the ionic radii and the hydration energy (ΔH_{hyd}) of the involved metal ions, where the $\Delta H_{hyd}{}^{Mn^{2+}}$ is the less negative one, with a tendency to be more endothermic from Mn to Ni. This feature can also be rationalized from the Pearson hard/soft acid-base approach. The Mn^{2+} specie is a hard acid, while Fe^{2+}, Co^{2+} and Ni^{2+} can be considered as borderlines. Since carbonate and phosphate are hard bases, the manganese will be more compatible with such anions favoring the formation of the Mn-based sidorenkite.

In order to explore the reaction time during the microwave processing, it was performed a few experiments at different processing times. A temperature of 210 °C was selected to prepare de Mn-sidorenkite $Na_3MnCO_3PO_4$. This temperature was selected due to the high crystallinity materials resulting from such condition. Figure 2 depicts the X-ray diffraction patterns acquired for the synthesized materials at 210 °C with 5, 10, 20, and 30 min of processing time. One can observe very similar diffraction patterns, indicating the formation of high crystalline $Na_3MnCO_3PO_4$ compounds for the applied experimental conditions. In addition, from these results, there are no significant structural differences associated with the processing times. This information reveals that only the 5 min reaction results

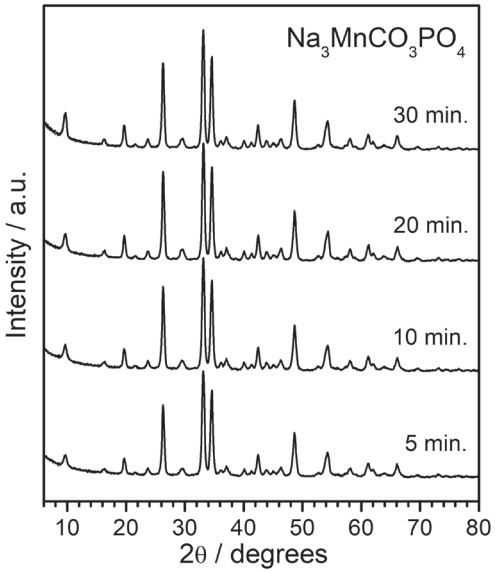

Figure 2. X-ray diffraction patterns of the $Na_3MnCO_3PO_4$ compounds obtained at 210 °C during different processing times: 5, 10, 20 and 30 min.

in a high ordered material, in an ultra-fast way, as compared with previously reported methods[30,35,38] which requires several hours or days.

The Rietveld refinement results (Table 1) also confirm that the synthesized materials have the same structure as the mineral form, according to the $P2_1/m$ space group, but with slightly different lattice parameters. These variations are predictable since the lattice parameters will be influenced by the transition metal ionic crystal radii, where Mn^{2+} (97 pm) > Fe^{2+} (92 pm) > Co^{2+} (88 pm) > Ni^{2+} (83 pm). This periodic trend along the series, combined to the severe distortion on the MO_6 octahedra, induce the observed lattice parameter and cell volume contractions. In addition, one can note significant variations of the unit cell parameters for the $Na_3MnCO_3PO_4$ compounds processed during 5 and 30 min. Since the 5 min processed material shows lattice parameters closer to the reference ones, one can infer that this compound is more structurally ordered, with less octahedra distortions, resulting in a high-quality material. Figure 3 shows the Rietveld refinement XRD patterns resulted from the $Na_3MnCO_3PO_4$ compounds obtained at 210 °C with 5 and 30 min of processing times.

As previously indicated by the analysis of Figure 1b, the $Na_3FeCO_3PO_4$ obtained at 210 °C is contaminated with Fe_3O_4. This feature was considered for Rietveld quantitative analysis, including such oxide as a second phase, resulting in the presence of 16% Fe_3O_4 (Figure S1, Supplementary Information (SI) section). In this case, the higher values of profile factor (R_p), weighted profile factor (R_{wp}) and residue (χ^2) as compared to the other materials (Table 1), can be attributed to the combination of both the presence of the iron oxide which induces asymmetries on the peaks, and due to the fluorescence effect of iron compounds when using CuKα radiation which increases the background signal.

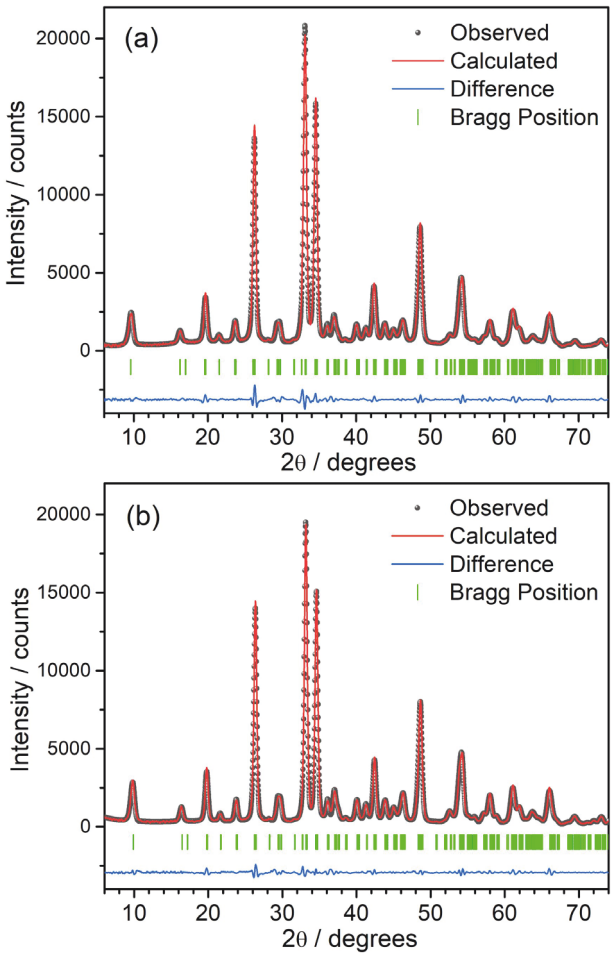

Figure 3. Rietveld refinements XRD patterns of $Na_3MnCO_3PO_4$ powders obtained from microwave processing at 210 °C during (a) 5 and (b) 30 min.

In addition, the Fe-based compound was also analyzed by Mössbauer spectroscopy in order to confirm the presence of different iron oxidation states. Figure 4 shows the acquired spectra and the resulting deconvolution analysis,

Table 1. Rietveld refinements results by using $P2_1/m$ space group for the synthesized carbonate-phosphates. The compound column indicates the evaluated material and the respective experimental conditions, temperature and processing time

Compound	a / Å	b / Å	c / Å	β / degree	V / Å^3	R_P / %	R_{WP} / %	χ^2
$Na_3MnCO_3PO_4$ (PDF 084-0023)	8.99	6.74	5.16	90.16	313.1	–	–	–
$Na_3MnCO_3PO_4$ 210 °C/5 min	8.97	6.96	5.19	90.27	306.0	5.12	6.70	3.80
$Na_3MnCO_3PO_4$ 210 °C/30 min	8.86	6.65	5.09	90.24	301.0	5.04	6.23	3.44
$Na_3FeCO_3PO_4$ 210 °C/30 min	8.98	6.64	5.16	89.76	308.7	22.2	20.8	9.85
$Na_3CoCO_3PO_4$ 210 °C/30 min	8.88	6.36	5.14	89.54	303.0	4.90	2.87	2.04
$Na_3NiCO_3PO_4$ 180 °C/30 min	8.81	6.58	5.11	89.28	297.0	5.86	4.47	2.66

a, b, c: cell dimensions; β: cell angle; V; cell volume; R_p: profile factor; R_{wp}: weighted profile factor; χ^2: residue.

which confirm the presence of both Fe^{2+} and Fe^{3+}. The Fe^{3+} content was estimated to be around 16 at.% by considering the specific spectrum area, as indicated on Table 2 which also includes the resulting hyperfine parameters. This 16 at.% value corresponds to around 8% of Fe_3O_4, an inverse spinel oxide $Fe^{III}(Fe^{II}Fe^{III})O_4$; a value which is significantly different from the 16% estimated by Rietveld analysis. This divergence can be explained based on the poor refinement resulted from the $Na_3FeCO_3PO_4$ diffraction pattern, with worse figures of merit values (R_p, R_{wp} and χ^2) and consequently a lower confidence level.

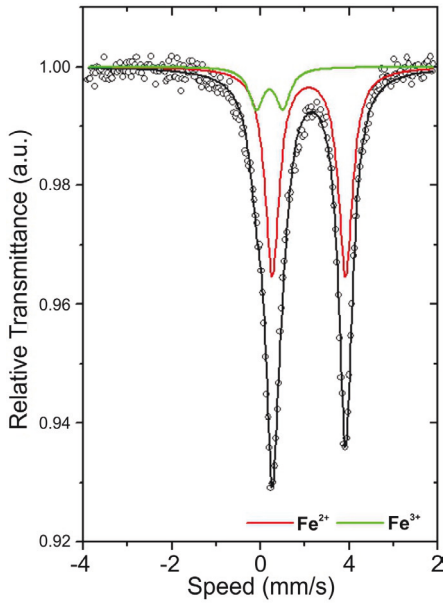

Figure 4. Room temperature ^{57}Fe Mössbauer spectra acquired for the $Na_3FeCO_3PO_4$ compound synthesized at 210 °C for 30 min.

Figure 5 shows the SEM images acquired for the Mn-based compounds obtained at the temperatures of 120, 150, 180 and 210 °C for 30 min processing. As previously indicated by the X-ray diffraction data (Figure 1a), the material resulted at 120 °C is constituted by a mixture of different phases including manganese carbonate and phosphates and the intended Mn-sidorenkite. The corresponding SEM image (Figure 5a) depicts an agglomeration of sheet-like structures, suggesting low-ordered materials with low-crystallinity in accordance with the XRD results. In contrast, Figures 5b-5d show finer crystallized materials, comprising irregular particles with a few hundred nanometers size. From XRD analysis (Figure 1a) these compounds were attributed to the $Na_3MnCO_3PO_4$ phase, where the higher temperature resulted in a high crystallinity material with well-formed particles. These results are in good agreement with previously reported results[11] for sidorenkite materials obtained by a hydrothermal method with 70 h of processing time.

The $Na_3MnCO_3PO_4$ obtained from the 5 min processing at 210 °C was also imaged by SEM and some representative images are presented on Figure 6. There can be observed that such material is constituted by an agglomeration of smaller particles when compared to the 30 min processed material. Figure 6b evidences the formation of nanoparticles typically ranging from 50 to 300 nm size. The evidenced nanoparticles habit is often reported for sidorenkite materials obtained by regular time-demanding hydrothermal methods. However, from a 5 min processing it is possible to prepare a polydisperse material with a smaller average particle size when compared with previous methods[9,11] which result in micrometer sized materials. It is worth comment that by using ion-battery active materials with reduced particle size, one can improve the ion insertion/extraction kinetics and consequentely the battery charge/discharge rate. These morphologycal features combined to a high-crystallinity, as evidenced by XRD, confirm that the developed methodology is efficient to prepare a high quality material in an ultra-fast way.

Figure 7 depicts the SEM images acquired for the sidorenkite-analogous compounds obtained by using Fe, Co and Ni. The $Na_3FeCO_3PO_4$ materials (Figures 7a and 7b) show similar features as compared to the Mn-based compounds. At both temperatures, 180 and 210 °C, the resulted compounds are constituted by irregular particles with a few hundred nanometers size. Moreover, the 210 °C processed material exhibits well-formed particles with rounded shape.

The SEM images acquired for the Co-based material, $Na_3CoCO_3PO_4$, are presented in Figures 7c and 7d. These results are particularly interesting because different morphologies were observed. The material obtained at 180 °C is formed by elongated particles with rod-shape ranging from hundred nanometers to one-micron length. Although the use of higher temperatures results in similar

Table 2. Mössbauer hyperfine parameters obtained for the iron-based sidorenkite compound, $Na_3FeCO_3PO_4$ synthesized at 210 °C/30 min processing time

Sample	Oxidation state	δ / (mm s^{-1})	Δ / (mm s^{-1})	Γ / (mm s^{-1})	Area / %
$Na_3FeCO_3PO_4$	Fe^{2+}	1.29 ± 0.05	1.64 ± 0.05	0.38 ± 0.05	84 ± 1
	Fe^{3+}	0.30 ± 0.05	0.60 ± 0.05	0.38 ± 0.05	16 ± 1

δ: isomer shift relative to α-Fe at room temperature; Δ: quadrupole shift; Γ: half-maximum line width; area: area of the spectrum component.

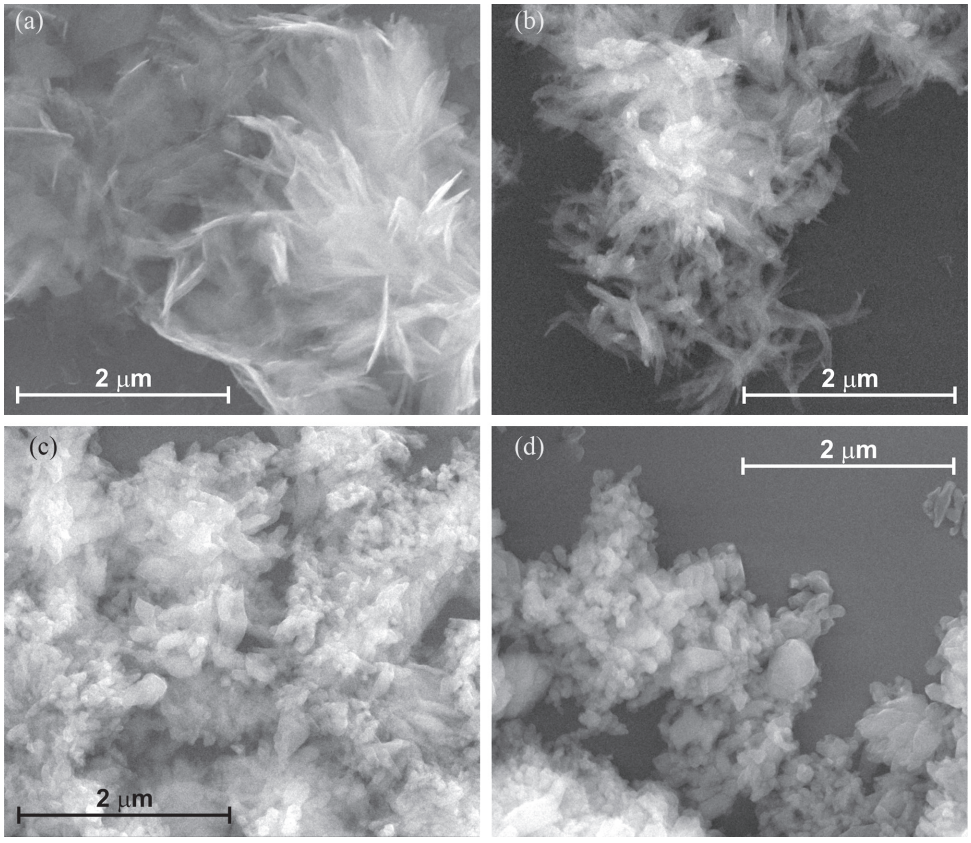

Figure 5. SEM images acquired for the Mn-based compounds obtained at the temperatures of (a) 120; (b) 150; (c) 180 and (d) 210 °C.

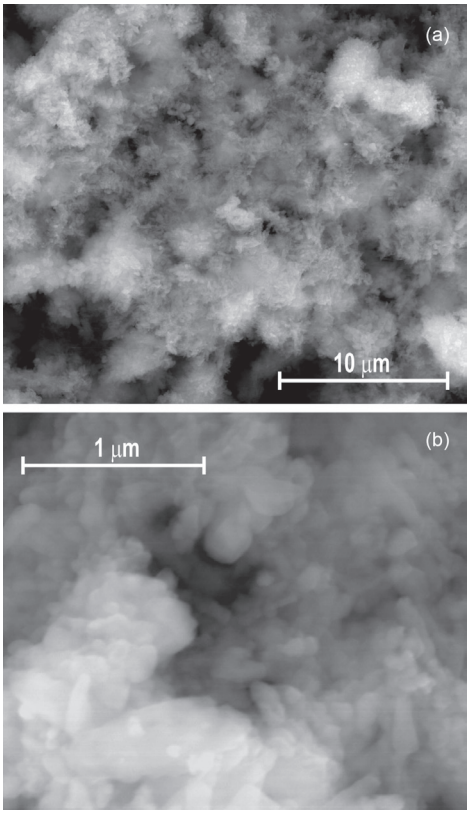

Figure 6. (a) SEM images acquired for the $Na_3MnCO_3PO_4$ compound synthesized at 210 °C with 5 min of processing time, detailed in (b).

morphologies for the other materials, in this case the 210 °C processed material shows a plate-like habit, often with a well-defined hexagonal shape with typical 500 nm length and 20 nm thick. This feature is uncommon since hexagonal crystals are not often originated from the monoclinic crystal system.

Figures 7e to 7g show the SEM images acquired for the $Na_3NiCO_3PO_4$ synthesized at 180 °C. These images evidence particles with a six-fold symmetry and a starfruit-like crystal shape, with typical size around 5 μm. Although the classical theory of nucleation and growth cannot be applied to explain the formation of this exotic crystal habit, this feature is particularly interesting and will be certainly explored in future works.

In addition, in order to evaluate the developed methodology to obtain the carbonate-phosphates, the prepared materials were characterized by thermogravimetric analysis. Combined to XRD this technique can be useful to probe the formation of byproducts during microwave processing. Figure 8a shows the thermogravimetric (TGA) curves with the weight-loss during the heating process up to 700 °C. The Mn- and Co-based materials obtained at 210 °C show very similar results with near 15% of weight-loss up to 600 °C, which is attributed to residual water and carbonate decomposition.[3] The Fe-based (210 °C) and the

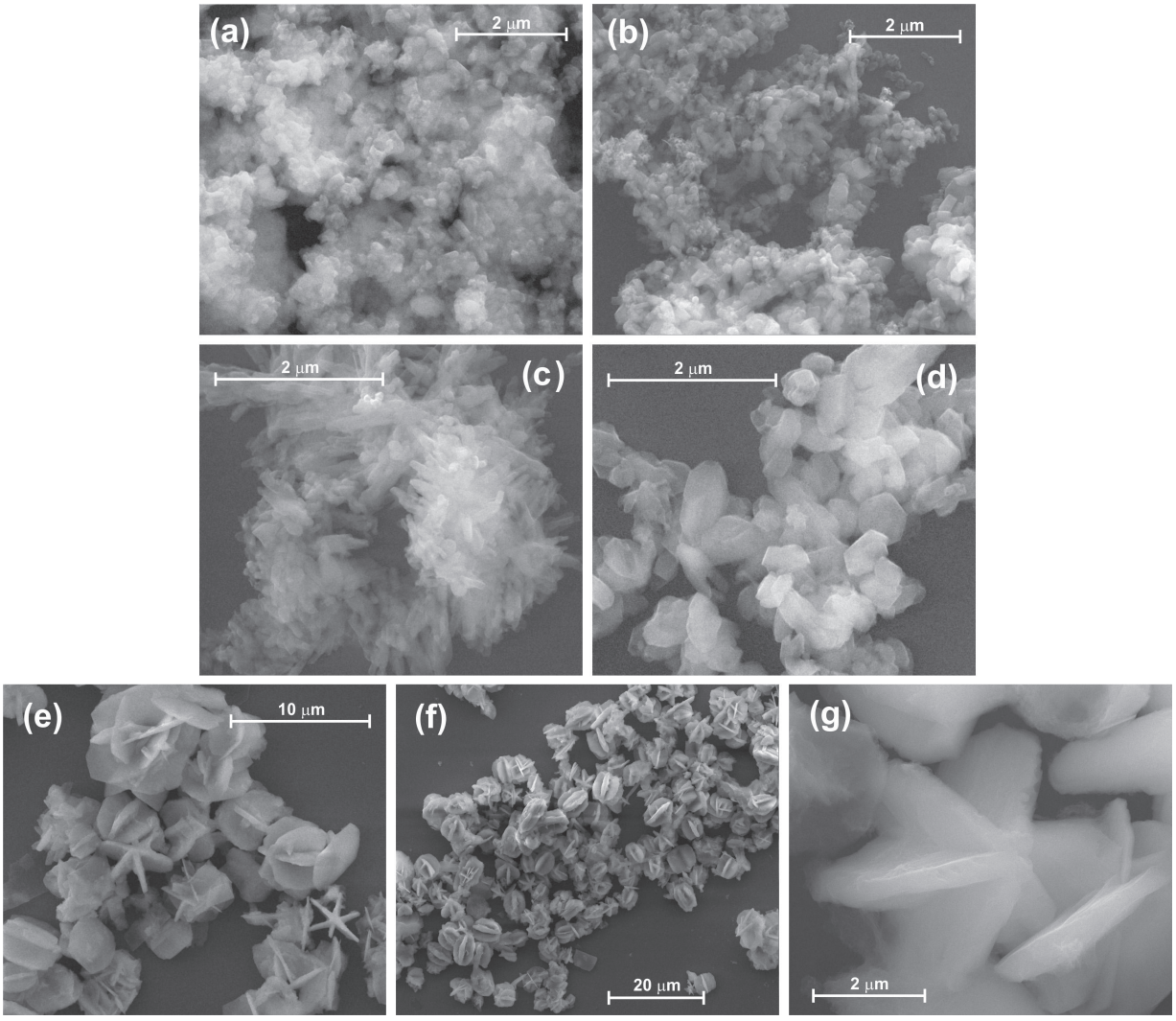

Figure 7. SEM images acquired for the sidorenkite-analogous compounds, $Na_3FeCO_3PO_4$ obtained at (a) 180 and (b) 210 °C; $Na_3CoCO_3PO_4$ prepared at (c) 180 and (d) 210 °C and (e-g) $Na_3NiCO_3PO_4$ starfruit shaped, obtained at 180 °C.

Ni-based (180 °C) compounds exhibit an additional weight-loss of 5% at temperatures below 500 °C. This behavior can be attributed to the presence of contaminants, mainly hydrated iron oxides and the layered nickel α-hydroxide, $Ni(OH)_{2-x}(A^{n-})_{x/n}.yH_2O$. These low crystallinity phases are not clearly revealed by XRD but can contribute to the background signal and broadening of specific diffraction peaks. The presence of the nickel α-hydroxide on the $Na_3NiCO_3PO_4$ materials is evidenced by the weak shoulders indicated by the red arrows in the Figure 1d. This contamination is strongly evidenced on the Ni-based material obtained at 210 °C, which shows significant weight-loss during heating from 200 to 400 °C attributed to the decomposition of hydroxide groups. Figures 8b, 8c and 8d show the results obtained from the TGA-MS analysis, where the ionic current for *m/z* 18 (H_2O), *m/z* 28 (CO) and *m/z* 44 (CO_2) evidence the hydroxide decomposition with water formation up to 400 °C, and the carbonate decomposition with CO and CO_2 formation around 600 °C.[41]

Although this work is mainly dedicated to report a new preparation methodology of a series of sidorenkite based materials ($Na_3MCO_3PO_4$), this relevant class of compounds can be applied to sodium insertion batteries. As a proof of application, preliminary tests were performed in order to demonstrate the electrochemical activity upon sodium extraction/insertion, during charge/discharge cycles. This class of compounds shows electrochemical activity in both aqueous and non-aqueous electrolytes. Although the best electrochemical response is obtained by using a sodium metal anode in a non-aqueous electrolyte, here it was used a sodium sulfate aqueous electrolyte with an insertion compound anode material, as previously described in the Experimental section. Figure 9 shows the charge discharge cycles obtained for the $Na_3MnCO_3PO_4$ compounds synthesized at 210 °C for 5 and 30 min of processing

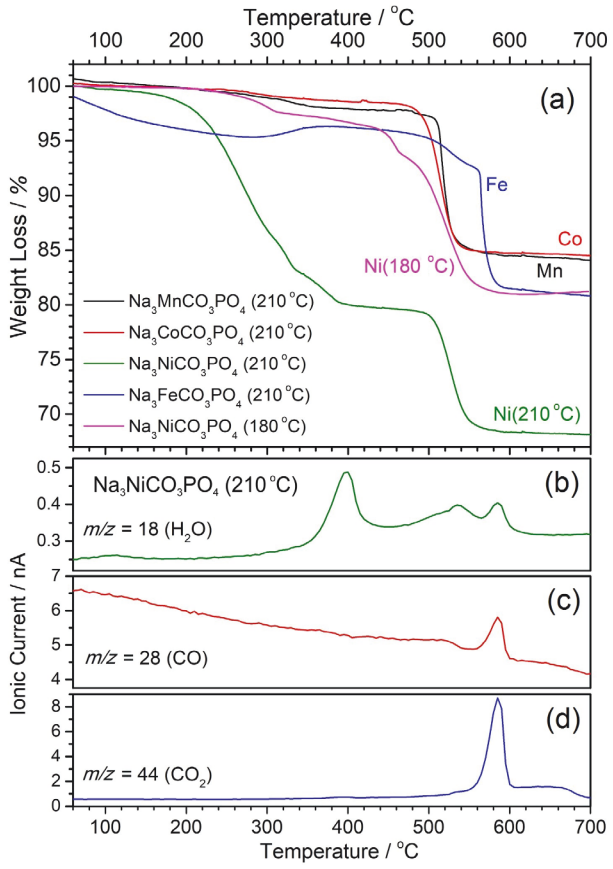

Figure 8. (a) Thermogravimetric analysis obtained for the sidorenkite analogous materials in argon atmosphere; (b-d) ionic currents resulted from coupled mass-spectrometry analysis for *m/z* 18, 28 and 44, respectively.

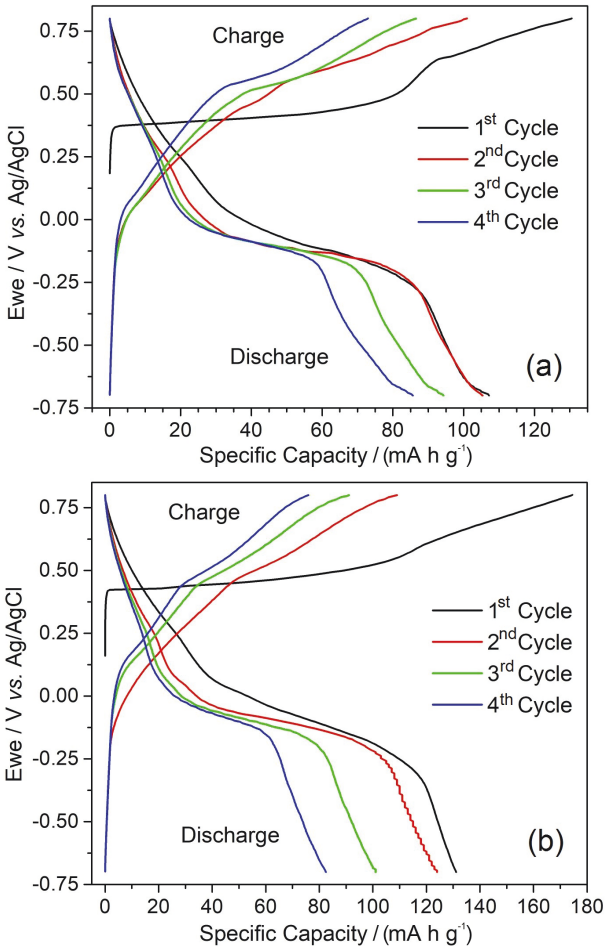

Figure 9. Charge/dicharge curves of sidorenkite $Na_3MnCO_3PO_4$, synthesized at 210 °C with (a) 5 and (b) 30 min processing times. The figures show the initial cycles obtained in aqueous electrolyte at C/20 rate.

time. During these initial cycles it was used a low charge/discharge rate of 20/C in order to attain the maximum specific capacity at such experimental conditions.

In the first cycle, the 5 min material exhibits charge and discharge capacities of 130 and 107 mA h g^{-1}, respectively. The 30 min compound shows charge and discharge capacity of 174 and 131 mA h g^{-1}. These values are consistent with the theoretical capacity of 191 mA h g^{-1}, which can be attained from insertion/extraction of two Na^+ ions by formula. These events are associated to the redox pairs Mn^{2+}/Mn^{3+} and Mn^{3+}/Mn^{4+}.[13] The use of sodium insertion anode material instead of sodium metal electrode may explain the irregular coulombic efficiency, what means the difference between the specific capacities of charge and discharge, observed for both materials noticed mainly in the first cycles. During these initial cycles one can observe a capacity fading to about 80-90 mA h g^{-1}. This capacity fading can be attributed to the material degradation during the charge/discharge process, as usually described in the literature.[14] However, an aqueous electrolyte is more adequate to the occurrence of the Mn^{2+}/Mn^{3+} redox pair, which results in only one active Na^+ ion *per* formula, resulting in a reversible capacity of 90 mA h g^{-1}.

Previously reported *in situ* X-ray diffraction studies[13] suggest that the sidorenkite and the analogous compounds show a reversible and topotactic sodium-insertion reaction with the formation of a solid solution. The sidorenkite insertion framework shows a Na(1) site, that is coordinated to seven oxygen atoms, and a Na(2) site, coordinated to six O atoms. The extraction process from these Na(1) and Na(2) ions is induced by the manganese oxidation, involving the redox pairs Mn^{3+}/Mn^{4+} and Mn^{2+}/Mn^{3+}, respectively.[13] Although, both Mn redox pairs are evidenced by the charge/discharge cycles, the Mn^{2+}/Mn^{3+} is the predominant event, as indicated by the smoothed plateau around 0 V at the discharge curve.

The discharge capacities obtained in different C-rates (C/20, C/4, C/2, C, 2.5C and 5C) for the two $Na_3MnCO_3PO_4$ materials with 5 and 30 min of proceesing times are exhibited in Figure 10. The results evidence a significant capacity fading when these materials are discharged at

high C-rates. The increase of the discharge rate from C/20 to 4C results in a capacity fading of 68% for both studied materials. This deleterious behavior is attributed to an intrinsic property of such class of compounds, the low electronic conductivity. Different from several metal oxides, these carbonate-phosphates show a poor electron conductivity.[14] The structural framework of these compounds are particularly favorable for a good ionic conduction. However, charge/discharge processes involve a mixed ionic and electronic transport, for both ion extraction/insertion and electron transport during the redox events of the manganese sites. This capacity evaluation at different discharge rates indicates that additional material modications could be necessary in order to improve power density. A usual chemical strategy involves a carbon coating process of the nanoparticulated materials, which can improve sigficantly the electronic conductivity of the composite electrodes.[42] It is possible to assume that the $Na_3MnCO_3PO_4$ synthesized for only 5 min of processing time shows a similar storage capacity when compared with the 30 min material. In addition, these results suggest that a carbon coating process could be used to improve the energy capacity of such class of compounds which could allow this material to supply enough energy density to face some sodium metal oxides that might operate with capacities as high as 80 mA h g^{-1} under more elevated current densities.[43] Moreover, this approach can be particularly adequate for materials with small particle size, as observed for the 5 min processed Mn-based compound.

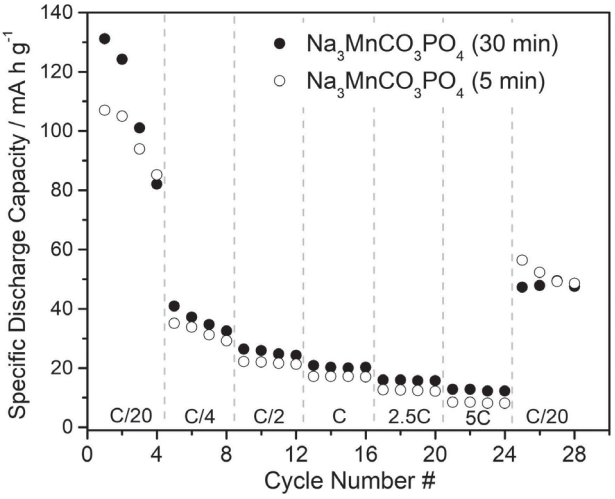

Figure 10. Specific discharge capacities obtained at different discharge rates from C/20 to 5C.

Conclusions

A microwave-assisted hydrothermal method for preparation of sodium-carbonate-phosphates was developed and applied for different compounds and processing parameters. By using this methodology, it was possible to prepare a Mn-sidorenkite $Na_3MnCO_3PO_4$ in as ultra-fast way, with only 5 min of processing time at 210 °C. Different materials based on first-row transition metals $Na_3MCO_3PO_4$ (M = Mn, Fe, Co, Ni) was also obtained with diverse nanoparticles size and shape, ranging from a few hundred nanometers to a few microns. Moreover, interesting morphologies or crystal habits resulted from such method, with the formation of rods, hexagonal plates and an exotic starfruit-shaped particle. It was also possible to determine the adequate experimental conditions to prepare high-quality materials, sometimes avoiding formation of side products. Preliminary electrochemical results indicate that the obtained Mn-based sidorenkite shows a good electrochemical performance with a reversible capacity of 65 mA h g^{-1} at low discharge rates. Although low, when compared with high energy lithium-battery materials, this capacity value is relevant since such compounds can be applied to low-cost stationary storage systems. However, this compound also shows low energy capacities when submitted to high discharge rates, suggesting that the poor electronic conductivity should be improved with additional preparation methods, such as a carbon coating. This approach can be particularly adequate for materials with small particle size, as observed for the 5 min processed Mn-based compound.

Thus, the developed microwave-assisted method can be used to synthesize high quality sodium-carbonate-phosphates with high crystallinity and reduced particle size. As compared to previously reported procedures, this new methodology is a very fast and energy saving approach, demanding shorter processing times.

Supplementary Information

Supplementary data (XRD refinements) are available free of charge at http://jbcs.sbq.org.br as PDF file.

Acknowledgments

The authors would like to acknowledge CAPES, PRPQ-UFMG and FAPEMIG (APQ-03567-16) for the financial support and the UFMG Microscopy Center for the technical support during electron microscopy experiments.

References

1. Goodenough, J. B.; Park, K.-S.; *J. Am. Chem. Soc.* **2013**, *135*, 1167.
2. Vliet, O. P. R.; Kruithof, T.; Turkenburg, W. C.; Faaij, A. P. C.; *J. Power Sources* **2010**, *195*, 6570.

3. Huang, W.; Zhou, J.; Li, B.; Ma, J.; Tao, S.; Xia, D.; Chu, W.; Wu, Z.; *Sci. Rep.* **2014**, *4*, 4188.
4. Zhou, D.; Huang, W.; Zhao, F.; *Solid State Ionics* **2018**, *322*, 18.
5. Minowa, H.; Yui, Y.; Ono, Y.; Hayashi, M.; Hayashi, K.; Kobayashi, R.; Takahashi, K. I.; *Solid State Ionics* **2014**, *262*, 216.
6. Zhou, Z.; Li, N.; Zhang, C.; Chen, X.; Xu, F.; Peng, C.; *Solid State Ionics* **2018**, *326*, 77.
7. Walczak, K.; Kulka, A.; Gedziorowski, B.; Gajewska, M.; *Solid State Ionics* **2018**, *319*, 186.
8. Zhu, L.; Li, Y.; Wang, J.; Zhu, X.; *Solid State Ionics* **2018**, *327*, 129.
9. Chen, H.; Hautier, G.; Ceder, G.; *J. Am. Chem. Soc.* **2012**, *134*, 19619.
10. Frost, R. L.; Lopez, A.; Scholz, R.; Belotti, F. M.; Xi, Y. F.; *Spectrochim. Acta, Part A* **2015**, *137*, 930.
11. Wang, C.; Sawicki, M.; Kaduk, J. A.; Shaw, L. L.; *J. Electrochem. Soc.* **2015**, *162*, 1601.
12. Hassanzadeh, N.; Sadrnezhaad, S. K.; Chen, G.; *Electrochim. Acta* **2016**, *208*, 188.
13. Chen, H.; Hao, Q.; Zivkovic, O.; Hautier, G.; Du, L.-S.; Tang, Y.; Hu, Y. Y.; Ma, X.; Grey, C. P.; Ceder, G.; *Chem. Mater.* **2013**, *25*, 2777.
14. Wang, C. L.; Sawicki, M.; Emani, S.; Liu, C. H.; Shaw, L. L.; *Electrochim. Acta* **2015**, *161*, 322.
15. Ellis, B. L.; Nazar, L. F.; *Curr. Opin. Solid State Mater. Sci.* **2012**, *16*, 168.
16. Yabuuchi, N.; Kubota, K.; Dahbi, M.; Komaba, S.; *Chem. Rev.* **2014**, *114*, 11636.
17. Komaba, S.; Murata, W.; Ishikawa, T.; Yabuuchi, N.; Ozeki, T.; Nakayama, T.; Ogata, A.; Gotoh, K.; Fujiwara, K.; *Adv. Funct. Mater.* **2011**, *21*, 3859.
18. Llave, E.; Borgel, V.; Park, K. J.; Hwang, J. Y.; Sun, Y. K.; Hartmann, P.; Chesneau, F. F.; Aurbach, D.; *ACS Appl. Mater. Interfaces* **2016**, *8*, 1867.
19. Ong, S. P.; Chevrier, V. L.; Hautier, G.; Jain, A.; Moore, C.; Kim, S.; Ma, X.; Ceder, G.; *Energy Environ. Sci.* **2011**, *4*, 3680.
20. Lee, D. H.; Xu, J.; Meng, Y. S.; *Phys. Chem. Chem. Phys.* **2013**, *15*, 3304.
21. Miao, X. W.; Yan, Y.; Wang, C. G.; Cui, L. L.; Fang, J. H.; Yang, G.; *J. Power Sources* **2014**, *247*, 219.
22. Wang, Y.; Chen, L.; Wang, Y.; Xia, Y.; *Electrochim. Acta* **2015**, *173*, 178.
23. Ji, H. M.; Yang, G.; Ni, H.; Roy, S.; Pinto, J.; Jiang, X. F.; *Electrochim. Acta* **2011**, *56*, 3093.
24. Chen, K.; Donahoe, A. C.; Noh, Y. D.; Li, K.; Komarneni, S.; Xue, D.; *Ceram. Int.* **2014**, *40*, 3155.
25. Yi, T. F.; Hao, C. L.; Yue, C. B.; Zhu, R. S.; Shu, J.; *Synth. Met.* **2009**, *159*, 1255.
26. Liu, C. L.; Chang, K. H.; Hu, C. C.; Wen, W. C.; *J. Power Sources* **2012**, *217*, 184.
27. Li, J. M.; Chang, K. H.; Wu, T. H.; Hu, C. C.; *J. Power Sources* **2013**, *224*, *59*.
28. Strachowski, T.; Grzanka, E.; Palosz, B.; Presz, B.; Slusarski, L.; Lojkowski, W.; *Solid State Phenom.* **2003**, *94*, 189.
29. Pazik, R.; Hreniak, D.; Strek, W.; *Mater. Res. Bull.* **2007**, *42*, 1188.
30. Wang, L. N.; Zhang, X.; Ma, Y.; Yang, M.; Qi, Y. X.; *Mater. Lett.* **2016**, *164*, 623.
31. Wang, X. F.; Jiang, H. Q.; Liu, Y. D.; Gao, M. D.; *Mater. Lett.* **2015**, *147*, 72.
32. Phuruangrat, A.; Kuntalue, B.; Thongtem, S.; Thongtem, T.; *Mater. Lett.* **2016**, *167*, 65.
33. Tang, M. X.; Yuan, A. B.; Xu, J. Q.; *Electrochim. Acta* **2015**, *166*, 244.
34. Li, L.; Seng, K. H.; Chen, Z. X.; Liu, H. K.; Nevirkovets, I. P.; Guo, Z. P.; *Electrochim. Acta* **2013**, *87*, 801.
35. Lin, H. Y.; Shih, C. Y.; *Catal. Surv. Asia* **2012**, *16*, 231.
36. Chen, R. R.; Wang, X.; Kong, X. Y.; *Mater. Lett.* **2014**, *120*, 76.
37. Cao, W.; *The Development and Application of Microwave Heating*; InTech: Rijeka, Croatia, 2012.
38. Ragupathy, P.; Vasan, H. N.; Munichandraiah, N.; *Mater. Chem. Phys.* **2010**, *124*, 870.
39. Balaji, S.; Mutharasu, D.; Sankara, S. N.; Ramanathan, K.; *Ionics* **2009**, *15*, 765.
40. Carvajal, J. R.; *Phys. B* **1993**, *192*, 55.
41. Rajamathi, M.; Subbanna, G. N.; Kamath, P. V.; *J. Mater. Chem.* **1997**, *7*, 2293.
42. Huang, G. Y.; Zheng, F. H.; Zhang, X. H.; Li, Q. Y.; Wang, H. Q.; *Electrochim. Acta* **2014**, *130*, 740.
43. Zhang, Z.; Hou, Z.; Li, X.; Liang, J.; Zhu, Y.; Qian, Y.; *J. Mater. Chem. A* **2016**, *4*, 856.

Submitted: January 25, 2019
Published online: July 11, 2019